# CDMA-based Acoustic Local Positioning System for Portable Devices with Multipath Cancellation

Fernando J. Álvarez[a,*], Teodoro Aguilera[a], Roberto López-Valcarce[b]

[a]*Department of Electrical Eng., Electronics and Automation, University of Extremadura, E-06006, Badajoz, Spain.*
[b]*Department of Signal Theory and Communications, University of Vigo, Vigo, E-36310, Spain,*

**Abstract**

This paper presents an acoustic local positioning system (ALPS) suitable for indoor positioning of portable devices such as smartphones or tablets, based on the transmission of high frequency CDMA-coded signals from a fixed network of beacons. The main novelty of the proposed ALPS is its capability to mitigate the effects of multipath propagation by performing an accurate estimation of the Line-of-Sight Time-of-Flights (LOS-TOF) through the Matching Pursuit algorithm. Signal detection, multipath cancellation and positioning estimation all take place within the portable device, which provides a graphical representation of the updated position in less than a second. The performance of the Matching Pursuit algorithm is analyzed in a real scenario and the results show that the proposed method is capable to retrieve the multipath-free System Availability under strong multipath conditions with SNR levels as low as 0 dB.

*Keywords:* Acoustic Local Positioning, Multipath Cancellation, CDMA-based Coding, Portable Devices

## 1. Introduction

The availability and computing power of smart devices such as phones and tablets have increased steadily in the last few years. These devices are also equipped with physical sensors such as an inertial motion unit, magnetic compass, light sensor, etc., that permit a better interaction of the user with the physical world. Of particular importance are Location Based Services (LBS)

*Corresponding author
*Email addresses:* fafranco@unex.es (Fernando J. Álvarez), teoaguibe@unex.es (Teodoro Aguilera), valcarce@gts.uvigo.es (Roberto López-Valcarce)

which are based upon knowledge of the users position in their environment. In today's common usage, LBS such as navigation guidance, restaurant finders, tourist guides, etc., are provided to the user as applications installed in their devices. Outdoor location is obtained by the device through the GPS receiver; however, it is well known that, due to the attenuation effects of roofs and walls as well as multipath propagation, GPS has very low accuracy or cannot fix a position at all in indoor environments, where much human activity takes place [1].

In order to extend the location availability to indoor environments, many technological possibilities have been proposed [2, 3]. However, most works that use a portable device as the mobile node of the positioning system can be classified into three main categories depending on their base technology, each one with its advantages and drawbacks with respect to the other two. The first category is formed by those systems that use the built-in accelerometer and magnetometer to perform Pedestrian Dead Reckoning (PDR) [4, 5, 6]. These systems do not need an external infrastructure, but they provide low precision location due to their inherent cumulative error. By using the accelerometer as a pedometer and the magnetometer as a heading provider compass, they typically achieve a precision of about 10% of the total traveled distance, although this value has been improved by combining the readings of the magnetometer with those of a gyroscope [7] or introducing Map Matching techniques [8].

In the second category we find all those systems based on the measurement of a Radio Frequency Received Signal Strength (RF-RSS). Unlike the previous case, these systems need an external infrastructure to generate the RF signals, but they can take advantage from already deployed WPAN [9, 10, 11] or WLAN [12, 13, 14, 15] transceivers. Due to the complex propagation of radio frequency signals indoors, RSS measurements are subject to large variability in this type of environments, resulting in typical positioning errors between one and a few meters. This poor accuracy has been improved by fusing RSS measurements with the information provided by the accelerometer [16, 17], both the accelerometer and the magnetometer [18, 19], the accelerometer and the gyroscope [20] or even the built-in barometer [21].

Finally, the third category, into which this work can be classified, comprises all those systems that measure the Time-of-Flight (TOF) of acoustic signals. Acoustic Local Positioning Systems (ALPS) can achieve centimetric precision thanks to the relatively low propagation speed of sound

in air, and they can also be easily implemented in portable devices since most of them are equipped with audio recording hardware. Systems as *Beep* [22], and a later evolution of this work [23], propose a centralized approach where a Personal Digital Assistant (PDA) emits short ultrasonic pulses that are detected by an array of six microphones, connected through a WLAN with a central process unit. These systems achieved positioning accuracies below 70 cm in 90% of cases, improving to 40 cm in positions away from walls and corners. A similar system is proposed in [24, 25], where a smartphone is used to emit short 21.5 kHz ultrasonic pulses detected by an array of four microphones. This centralized system achieved errors below 10 cm by minimizing a positioning cost function. A different approach is proposed in the *BeepBeep* ranging system [26], where the authors present a two-way sensing technique to estimate the relative distance between a PDA and a smartphone. By measuring the TOF of chirp signals with frequencies between 2 and 6 kHz, this system achieved positioning errors of 5 cm for distances below 4 m. Later, several works benefited from the *BeepBeep* ranging technique to develop different relative indoor positioning systems among smartphones and tablets [27, 28, 29], reporting average positioning errors between 10 and 30 cm.

The main disadvantage of all these systems is their limited update rate, due to the need to avoid signal collisions, and robustness against in-band noise. The current signal processing capabilities of smartphones and tablets [30] allow for more efficient CDMA-based systems, in which all signals can be simultaneously emitted with low energy. The advantages of this multiple access scheme are well known and have been already exploited in the design of general-purpose ALPS [31, 32, 33, 34]. However, the use of longer and simultaneous emissions aggravates the pernicious effect of phenomena such as multipath propagation. Most of the previous works do not include multipath-affected areas in their experimental test regions, and there are only a few authors that openly admit a clear deterioration of their system performance in these critical areas [23, 26, 27]. Very recently, some works have appeared in the field of ALPS which pay special attention to the development of multipath cancellation strategies. This is, for example, the case of [35], where the authors propose a TDMA-based system that performs the cyclic emission of pseudo-noise to locate a smart portable device. This system discards the arrival of reflected echoes by making use of sliding windows based on the a priori known features of the cyclic emission. Also, in [36] an iterative Peak

Matching algorithm is proposed to cancel the effect of multipath in the auto-calibration process of a wireless network of acoustic sensors that perform the emission of Maximum length sequences. Once the direct path TOFs have been identified with the help of this algorithm, all ranges between sensors are estimated by combining multidimensional scaling (MDS) with the above mentioned BeepBeep technique.

This work presents a CDMA-based ALPS, which provides indoor localization for portable devices that acquire the coded signals simultaneously emitted from a set of fixed beacons, and perform all the necessary computations without the participation of any external processing unit. An essential feature of this ALPS is its design for CDMA-positioning, including the acoustic signal processing for robust TOF estimation and a multipath compensation technique that notably improves the system performance in those areas affected by this phenomenon. This technique is based on the Matching Pursuit algorithm, which has been proven to accurately detect direct transmission path signals which are highly attenuated in CDMA-based systems [37, 38]. This capability has been recently investigated by the authors in the context of a broadband ALPS [39], a preliminary work where the image method proposed by Allen and Berkley [40] was used to model the acoustic behavior of a small room and simulate the system performance. This current work presents the materialization in a practical ALPS of the model described in [39], an objective that entails the following challenges:

- Designing the emission architecture, including beacons, driving electronics and positioning signals.
- Developing a positioning application for the portable device, including a signal detection stage, a Gauss-Newton positioning algorithm and the graphical representation of the results through a user-friendly interface.
- Incorporating the Matching Pursuit algorithm into this positioning application, adapting the programming strategies to the particularities of the portable device processor.
- Testing the system in real scenario, under strong multipath conditions and with different levels of noise, to validate the design.

The rest of the paper is organized as follows. Section 2 presents a complete description of the acoustic positioning system, including design aspects, physical properties of the transducers and electronics, and positioning strategy and signals. In Section 3, the effect of multipath propagation on the performance of an ALPS is described, and a solution based on the Matching Pursuit channel estimation algorithm is proposed. Section 4 describes the practical implementation of this solution in the portable device and Section 5 contains the experimental evaluation of the positioning system, paying special attention to its performance with respect to multipath cancellation. Finally, the main conclusions of this work are drawn and discussed in Section 6.

## 2. Description of the Acoustic Local Positioning System

a)


b)

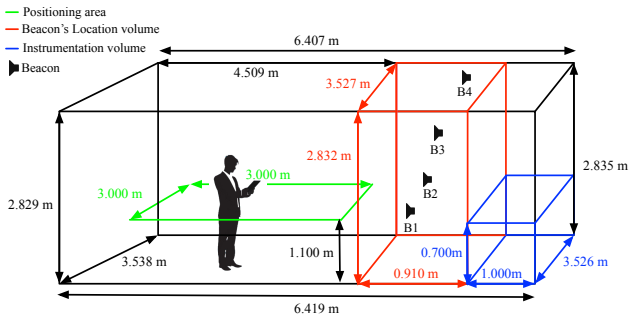


| Beacon | x (m) | y (m) | z (m) |
|---|---|---|---|
| B1 | 3.526 | 5.000 | 0.700 |
| B2 | 1.756 | 4.517 | 1.763 |
| B3 | 3.526 | 4.509 | 2.835 |
| B4 | 0.000 | 4.509 | 2.743 |

Figure 1: Schematic representation of the acoustic positioning system proposed in this work. Beacon coordinates are measured with $\pm 1$ mm accuracy by using a laser rangefinder (Bosch GLM80).

The general arrangement of the acoustic positioning system proposed in this work is shown

in Fig. 1a. Four acoustic emitting beacons are placed in different positions inside a box-shaped room, whose dimensions can also be seen in Fig. 1b. These beacons are close to the wall which is farthest from the entrance and with their acoustic axis perpendicular to it, thus allowing optimal signal reception to those users facing this wall. This configuration is particularly useful for certain types of LBS such as those designed to provide information to the visitors of a museum whose exhibits are shown in a single wall (as long as there are no occlusions of the direct propagation path). Beacons final emplacement inside the beacon's location volume has been determined by conducting a metahuristic search to minimize the Position Dilution of Precision (PDOP) in the entire positioning area. A mean PDOP value of 5.07 has been obtained with the configuration shown in Fig. 1b, which corresponds to a class 3 or *Good* rating according to [41].

The beacons are programmed to simultaneously emit encoded acoustic signals that are detected by the receiver (a portable device) carried by the user. This device processes the received signal, determines the TOF from each beacon (within an unknown time base), and computes an estimate of its position. Figure 2 shows the acoustic impulse responses of the room in the center of the positioning area for every beacon, obtained by means of the MLS technique [42]. The presence of strong multipath propagation is evident in this figure, where direct paths, early reflections and late-field reverberations can be clearly identified. A 60 dB reverberation time of $T_{60} \approx 1$s is obtained from these responses.

The following subsections provide detailed information about the most relevant aspects of this ALPS, namely, the emitting and receiving transducers with their corresponding electronics, the acoustic positioning signals and the positioning strategy.

### *2.1. Emitter and receiver architecture*

The emission architecture is easily illustrated with the help of Fig. 3. The coded signals are synthesized using a Virtex 5 FPGA-based board, which has been programmed to simultaneously generate pseudoramdom emissions every 35 ms. These digital signals are fed into a couple of double digital-to-analog converter modules (Digilent PmodDA2), and the analog outputs are high-pass filtered to remove the DC offset. Finally, these signals are carried into a pair of two-channel audio amplifiers (Philips TDA8920BTH), powered with a DC source to drive a set of four high-

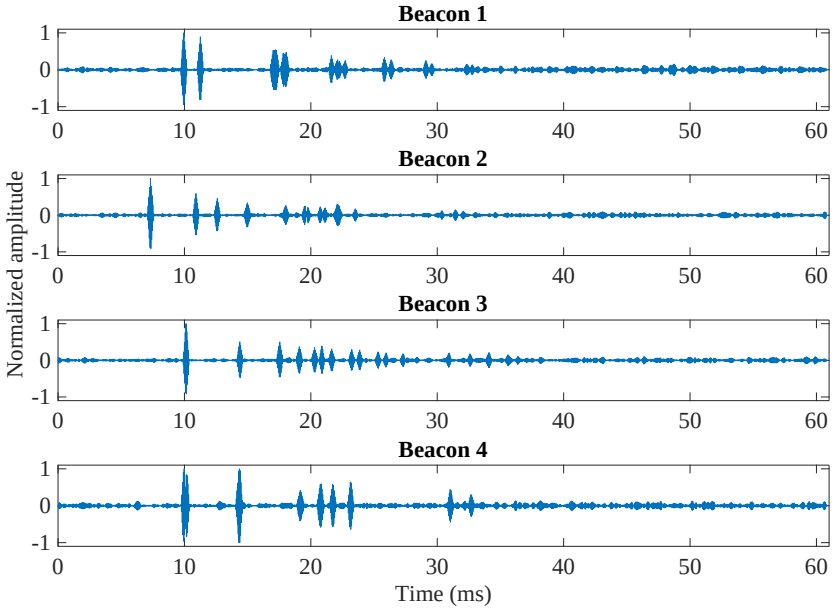


Figure 2: Acoustic impulse responses of the room in the center of the positioning area for every beacon.

frequency speakers (Visaton CP13). Figures 4a, 4b and 4c show respectively a picture of the speaker, its acoustic directivity pattern and the frequency response, as provided by the manufacturer.

As stated before, the receiver module of the ALPS proposed in this work is a portable device (iPad Air 2). The acoustic signal composed by the positioning codes is detected by the built-in microphone of this device and then processed by its internal processor (A8X). Fig. 5 shows the frequency response of this microphone, experimentally obtained in our laboratory (blue dots), and that of an IIR filter of order 50 designed to simulate the LPS behavior prior to the experimental study (red line).

### *2.2. Positioning signals*

In order to identify each beacon individually, their positioning signals are encoded with a particular, Binary-Phase Shift Keying (BPSK) modulated, pseudorandom Kasami code. These codes improve the cross-correlation properties of Gold sequences (and therefore that of Maximum Length sequences) at the expense of reducing the number of sequences with these properties from

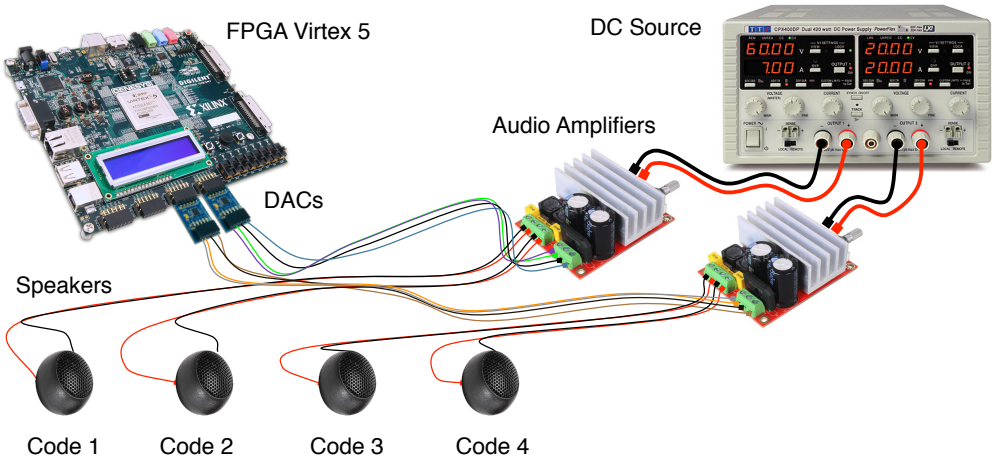


Figure 3: Connection diagram of the emission architecture of the ALPS.

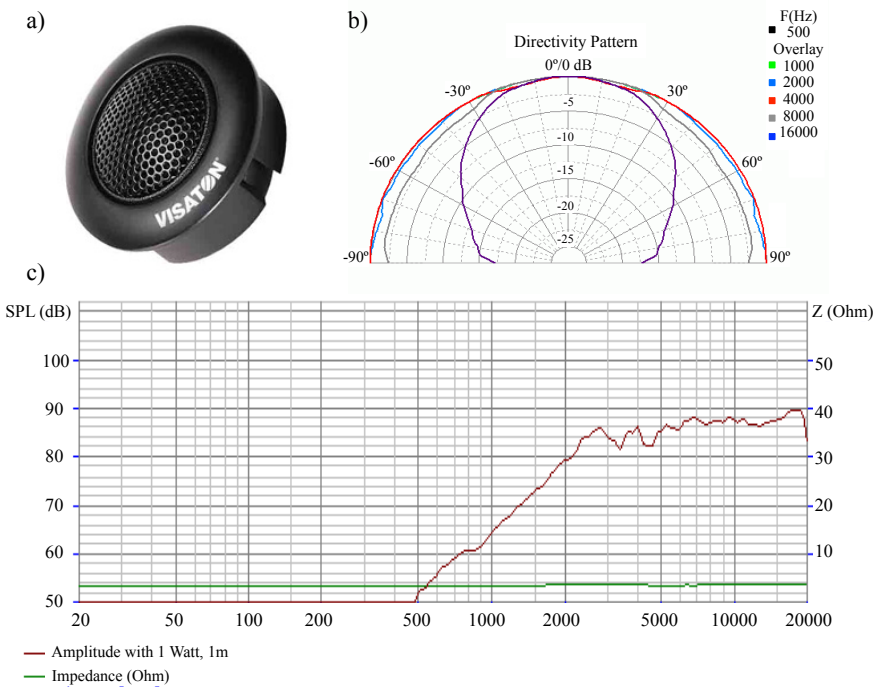


Figure 4: a) Picture, b) directivity pattern, and c) frequency response of the CP13 Visaton speaker, as provided by the manufacturer.

$2^N + 1$ to $2^{N/2}$, with $L = 2^N - 1$ being the length of the sequences. Thus, they represent a good choice if the number of sequences needed is not too large, and for this reason they have been commonly used in the design of broadband general-purpose ALPS [34, 43]. Although these correlation

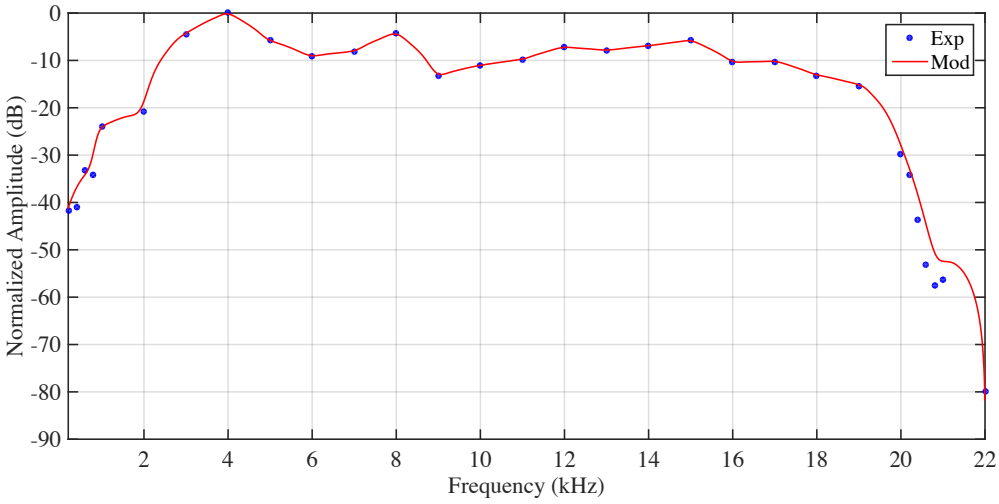


Figure 5: Frequency response of the receiver module (iPad microphone) experimentally obtained in our laboratory.

properties have been improved by the use of Interference Free Window Sequences [44], these latter impose a taught constraint on the geometrical distribution of the emitters that ultimately deteriorates the system PDOP. Also, recent works have demonstrated a better Doppler-shift resilience of Kasami codes against ideal correlation codes such as Loosely Synchronous and Complementary Set of Sequences [45].

Next, we address the choice of three key parameters: carrier frequency, bit duration and length of the positioning codes. The carrier frequency must lie within the combined bandwidth of the emitting and the receiving transducers, extending from 2 to 20 kHz approximately. This frequency should be high enough as to avoid causing excessive disturbance while maintaining a reasonably wide directivity. A value of $F_c = 16$ kHz has been finally chosen as a good compromise between both constraints. The bit interval, i.e, the number of carrier cycles per bit ($N_C$) determines the signal bandwidth, but also the spatial resolution of the system which is roughly given by $c/(F_c \times N_C)$, $c$ being the speed of sound in air. We opted for $N_C = 1$ to keep this resolution as low as possible ($\approx 2$ cm), causing 35% of the emitted energy to be filtered away by the receiver because of the relatively wide signal bandwidth. Nevertheless, despite this significant loss of energy, the correlation properties of the filtered codes are not severely degraded as will be seen below.

Regarding the Kasami code length, we considered 63-bit and 255-bit signals for the emissions.

Although longer codes provide larger correlation peaks, this is also true for the secondary echoes and therefore there is not actual improvement in the process of discriminating between the main and the secondary peaks, as far as all of them arise above the noise level. The main advantage of using longer codes is that less energy is necessary to obtain similar performance, but the price to pay is having to process longer data streams. Since a reduced computational load is a primary objective of the proposed system to achieve real-time operation, we finally settled for the relatively short 63-bit Kasami codes.

To further study the effect of the limited bandwidth on the ranging signals, we emitted a coded signal from a single beacon and received it with the iPad placed at a distance of 0.7 m over its acoustic axis. Figures 6a and 6b depict the emitted pattern and the received signal respectively, clearly showing the filtering effects caused by the reduced receiver's bandwidth. The aperiodic correlation of the received signal with the emitted code is shown in Fig. 6c, along with the ideal correlation. The degradation in the correlation shape, especially evidenced in the ringing after the first correlation peak, is caused by the limited bandwidth of the acoustic channel as well as the imperfect spatial alignment of emitter and receiver [46]. Finally, Fig. 6d shows the cross-correlation of the ideal and actual received signal with the pseudo-orthogonal code assigned to a different beacon.

### *2.3. Estimation of the receiver's position*

Once the processor produces valid TOFs from the respective beacons (although referred to an unknown time base), hyperbolic multilateration is used by the receiver to estimate its position [47]. This technique involves measuring the Time-Difference-of-Flight (TDOF) between the first detected signal, emitted by the nearest beacon (BN) and the other signals detected subsequently, emitted by the remaining beacons. The locus of the points that measure the same TDOF between the nearest beacon and a second one (B1) define a hyperboloid whose focal points are those beacons. A second hyperboloid intersecting the first one can be obtained from the TDOF between the closest beacon and a third one (B2). With the help of a fourth beacon (B3), an additional hyperboloid intersecting the previous two in a single point can be obtained to fully determine the user's position. Fig. 7 shows a 2D representation of the multilateration technique.

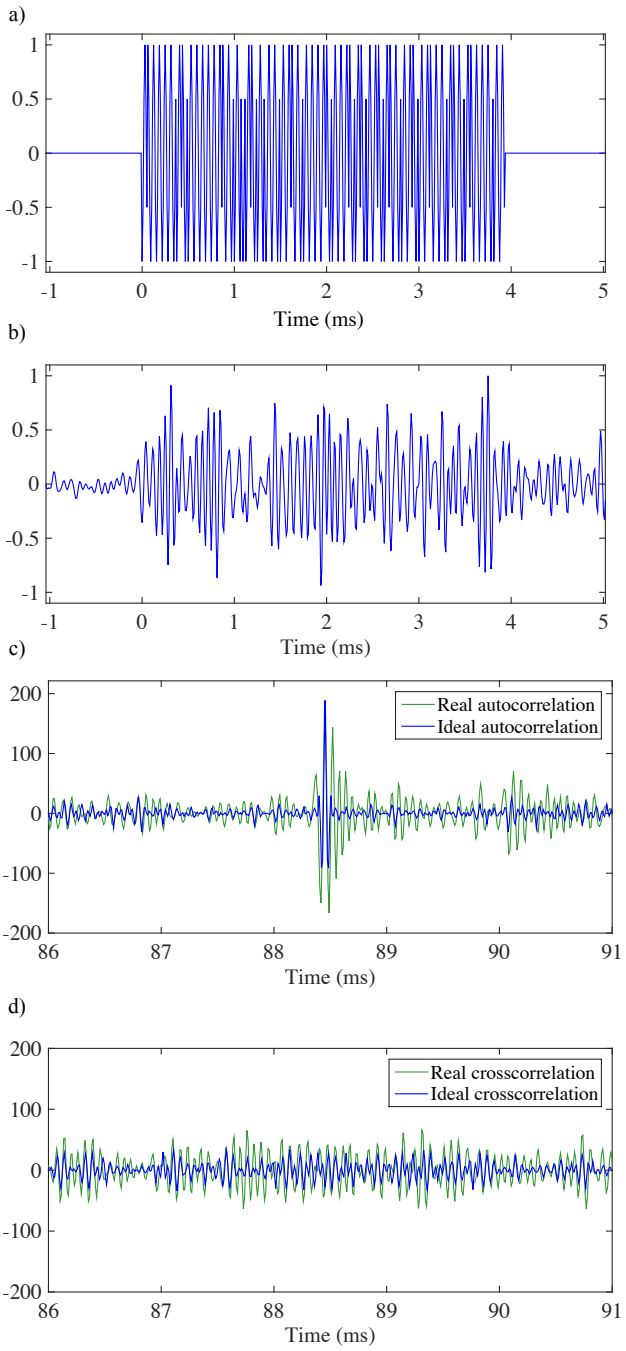


Figure 6: Emitted a) and received b) signals, from only one beacon. Ideal versus real autocorrelation c) and ideal versus real crosscorrelation d) of the emitted codes.

The user's position can be algebraically obtained either by solving a system of nonlinear equations with four beacons or a system of linearized equations obtained with the participation of

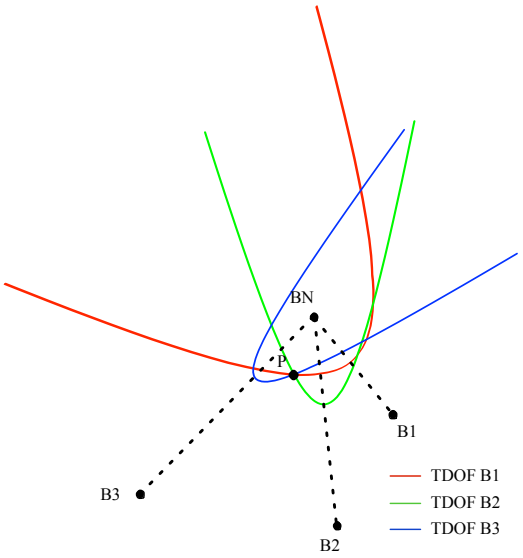


Figure 7: Planar representation of the multilateration technique.

an extra beacon. Nevertheless, the presence of errors in the differential distances measurements has as a consequence that the hyperboloids do not longer intersect in a single point, and the position must be resolved as a non-linear least squares problem. Our proposal makes use of the Gauss-Newton optimization algorithm to iteratively resolve this position, providing high robustness without adding any new beacon at the expense of increasing the computational complexity. If we define the differential distance between beacon $\mathbf{b}_i = (x_i, y_i, z_i)$ and the nearest beacon $\mathbf{b}_n = (x_n, y_n, z_n)$ from the estimated user's position $\mathbf{p} = (x, y, z)$ as,

$$\hat{\Delta} r_i(\mathbf{p}) = \|\mathbf{b}_i - \mathbf{p}\| - \|\mathbf{b}_n - \mathbf{p}\| \quad \text{for } i = 1,2,3. \tag{1}$$

and the same distances obtained from the measured TDOFs as,

$$\Delta r_i = c \cdot \text{TDOF}_i, \tag{2}$$

then we can build the objective function to be minimized as,

$$F(\mathbf{p}) = \sum_{i=1}^{3} [f_i(\mathbf{p})]^2, \tag{3}$$

where $f_i(\mathbf{p}) = \hat{\Delta} r_i(\mathbf{p}) - \Delta r_i$.

Approximate solutions to the minimization of (3) can be obtained by different ways, as discussed in [48], in order to initialize the Gauss-Newton iteration. However, when the dimensions of the room are not too large, a computationally cheaper option is to simply take the center of the room as the initial position estimate $\mathbf{p}_0 = (x_0, y_0, z_0)$. Starting from this position, subsequent estimates of this parameter can be obtained by means of the recursive relation:

$$\mathbf{p}_{k+1} = \mathbf{p}_k - \mathbf{J}_\mathbf{f}(\mathbf{p}_k)^{-1}\mathbf{f}(\mathbf{p}_k), \tag{4}$$

where $\mathbf{f}(\mathbf{p}_k) = (f_1, f_2, f_3)$ and $\mathbf{J}_\mathbf{f}(\mathbf{p}_k)$ is the Jacobian matrix of $\mathbf{f}$ with respect to $\mathbf{p}_k$, i.e.,

$$\mathbf{J}_\mathbf{f}(\mathbf{p}_k) = \begin{pmatrix} \dfrac{\partial f_1}{\partial x} & \dfrac{\partial f_1}{\partial y} & \dfrac{\partial f_1}{\partial z} \\ \dfrac{\partial f_2}{\partial x} & \dfrac{\partial f_2}{\partial y} & \dfrac{\partial f_2}{\partial z} \\ \dfrac{\partial f_3}{\partial x} & \dfrac{\partial f_3}{\partial y} & \dfrac{\partial f_3}{\partial z} \end{pmatrix}. \tag{5}$$

Since our positioning system operates without time synchronization and uses exactly the minimum required number of beacons, TOF outliers cannot be detected by redundancy techniques, such as the parity space [49]. Instead, we have implemented a straightforward method based in a temporal filter which discards TOF values which deviate largely from previously determined ones. Although simple, this technique permits to eliminate most instances of outliers in the computed position.

## 3. Multipath cancellation algorithm

Multipath propagation is a main cause of degradation in the performance of broadband ALPS. The effect of this phenomenon is critical near room walls and corners, where the strongly reflected signals interfere with the Line-of-Sight (LOS) emissions and deteriorate the ideal correlation properties of these emissions. As a direct consequence of this deterioration, the largest correlation peaks obtained by matched filtering at the receiver do not always correspond to the instant of arrival of the LOS emissions.

*3.1. Sparse channel estimation*

The problem described above can be overcome by performing a precise estimation of the channel impulse response. Note that the time of occurrence of the first coefficient in this estimated response represents the desired TOF, since in an acoustic LPS a Line-of-Sight path between the beacons and the receiver must always be assured. We consider first the case of a single channel composed by one beacon and one receiver. In this situation, when the received signal $r(t)$ is digitized at a sampling rate $F_s = 1/T_s$ and if we assume a multipath spread of $N_s \times T_s$ seconds, this signal can be represented by,

$$\mathbf{r} = \mathbf{E}\mathbf{h} + \mathbf{n}, \tag{6}$$

where $\mathbf{r} = [r[N_s], r[N_s+1], \cdots, r[N_s+p-1]]^T \in \mathbb{R}^{p\times 1}$ is a vector containing $p$ samples of the received signal, $\mathbf{h} = [h_1, h_2, \cdots, h_{N_s}]^T \in \mathbb{R}^{N_s\times 1}$ is the channel coefficient vector, $\mathbf{n} = [n[1], n[2], \cdots, n[p]]^T \in \mathbb{R}^{p\times 1}$ is a vector of zero-mean white Gaussian noise samples and,

$$\mathbf{E} = \begin{bmatrix} e[N_s] & e[N_s-1] & \cdots & e[1] \\ e[N_s+1] & e[N_s] & \cdots & e[2] \\ e[N_s+2] & e[N_s+1] & \cdots & e[3] \\ \vdots & \vdots & \cdots & \vdots \\ e[N_s+p-1] & e[N_s+p-2] & \cdots & e[p] \end{bmatrix} \in \mathbb{R}^{p\times N_s},$$

is the characteristic signal matrix containing samples $e[n]$ of the beacon's emitted signal. As it is well known, the maximum likelihood (ML) estimate for the channel coefficients is the solution to the following minimization problem,

$$\hat{\mathbf{h}} = \underset{\mathbf{h}}{\operatorname{argmin}} \left\{ \|\mathbf{r} - \mathbf{E}\mathbf{h}\|^2 \right\}, \tag{7}$$

whose optimal solution is given by the Least Squares (LS) estimate

$$\hat{\mathbf{h}} = (\mathbf{E}^H\mathbf{E})^{-1}\mathbf{E}^H\mathbf{r}. \tag{8}$$

Note that the pseudo-inverse of the characteristic signal matrix $(\mathbf{E}^H\mathbf{E})^{-1}\mathbf{E}^H$ can be precomputed to facilitate the ML channel estimation defined by (8), since this matrix is known in advance. However, considering that the number of samples in an ALPS channel response is typically of several thousands, it is clear that the ML solution is not a feasible implementation for a real-time operating system. This situation is even more problematic if multiple channels are to be estimated jointly.

Here we explore the Matching Pursuit (MP) channel estimation algorithm as an alternative to the ML solution. This algorithm provides a low complexity approximation to the ML solution for sparse channels [38], i.e., channels where the number of coefficients with non-negligible magnitude is much lower than the total number of coefficients. The MP algorithm minimizes (7) iteratively, one estimated channel coefficient $\hat{h}_{q_j}$ at a time, using a greedy approach in which the detected path index $q_j$ and $\hat{h}_{q_j}$ are selected such that the decrease in (7) at each stage $j$ is the largest possible [37]. That is, multipath signal components are estimated via successive interference cancellation. For $j = 1, 2, \ldots, N_f$,

$$q_j = \underset{i \neq q_1, \ldots, q_{j-1}}{\operatorname{argmax}} \left\{ \frac{\left|\mathbf{E}_i^H \mathbf{r}^j\right|^2}{\|\mathbf{E}_i\|^2} \right\}, \tag{9}$$

and

$$\hat{h}_{q_j} = \frac{\mathbf{E}_{q_j}^H \mathbf{r}^j}{\left\|\mathbf{E}_{q_j}\right\|^2}, \tag{10}$$

with

$$\mathbf{r}^{j+1} = \mathbf{r}^j - \frac{\mathbf{E}_{q_j}^H \mathbf{r}^j \mathbf{E}_{q_j}}{\left\|\mathbf{E}_{q_j}\right\|^2}, \tag{11}$$

where $\mathbf{E}_i$ represents the $i-th$ column vector of matrix $\mathbf{E}$ and $\mathbf{r}^1 = \mathbf{r}$. The algorithm concludes after stage $j = N_f$. Eq. (6) can be easily extended to account for $L$ simultaneous channels as,

$$\mathbf{r} = \sum_{l=1}^{L} \mathbf{E}^l \mathbf{h}^l + \mathbf{n}, \tag{12}$$

where $\mathbf{h}^l$ is the $l-th$ channel coefficient vector and $\mathbf{E}^l$ is the characteristic signal matrix of the $l-th$ beacon. In this case, every new iteration of the MP algorithm computes Eqs. (9) and (10) $L$ times, and only the largest coefficient $\hat{h}^l_{q_j}$ is stored. Next, the newly estimated signal $\hat{h}^l_{q_j}\mathbf{E}^l_{q_j}$ is substracted from the current residue $\mathbf{r}^j$ to obtain the updated signal $\mathbf{r}^{j+1}$ as indicated by (11).

### *3.2. LOS-TOFs calculation*

Once we have seen that the TOF of the Line-of-Sight emission can be derived from a precise estimation of the channel impulse response, it is necessary to determine the number of coefficients to be calculated by the MP algorithm. Clearly, in order to minimize the computational load of the MP algorithm this number must be as low as possible but, on the other hand, it should be large enough as to be useful in a wide variety of different situations. The simulation analysis conducted by the authors in [39] confirmed that a total number of four coefficients (one per channel) is enough to estimate the LOS-TOFs in the trivial case of very weak multipath interference. This situation is depicted in Fig. 8, where it can be seen that the four channels LOS-TOFs are estimated with errors below 0.002 ms. However, this is not possible with very strong multipath interference that may cause the appearance of larger coefficients in the impulse response than those associated with the Line-of-Sight paths. In this case, the results show that a minimum of three coefficients estimated per channel (for a total minimum of 12 coefficients) can assure a correct estimation of the desired TOFs. This new situation is depicted in Fig. 9. The problem now is that, if a large number of coefficients is calculated in the case of weak multipath interference or not interference at all, some spurious coefficients may appear before the Line-of-Sight path coefficient. This problem can be easily solved by establishing a detection threshold below which all calculated coefficients are discarded as LOS-TOF candidates. Fig. 10 represents the same situation as that in Fig. 8, but when the MP algorithm is forced to calculate a minimum of three coefficients per channel. As can be seen, in this case, a detection threshold chosen as half the value of the largest coefficient estimated in each channel (green dashed line), is above all spurious coefficients thus allowing the correct estimation of the LOS-TOFs.

To summarize, the proposed method makes use of the multichannel MP algorithm to first calculate at least three coefficients of every channel impulse response, and then estimates the TOF

of the Line-of-Sight path by detecting the time of occurrence of the first coefficient whose value is above half the value of the largest coefficient estimated in each channel.

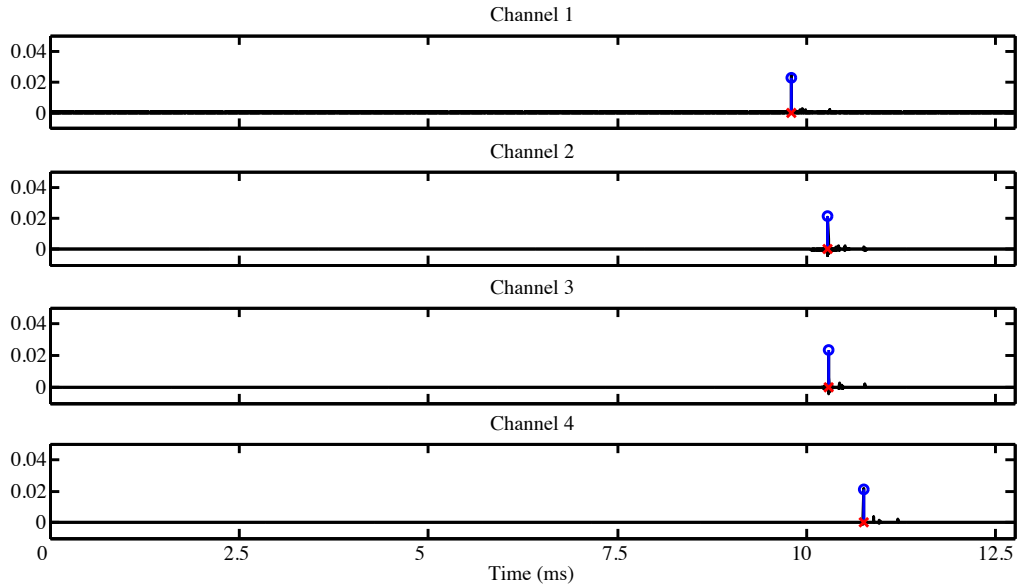


Figure 8: Impulsive response (black line), estimated coefficients (blue circles) and estimated LOS-TOF (red cross) under weak multipath interference conditions. The MP algorithm was programmed to calculate a total number of four coefficients, finding one per channel in these conditions.

## 4. Real-time implementation in the portable device

The implementation of the ALPS reception module has been performed on a last generation iPad (iPad Air 2), which is equipped with 2 GB of LPDDR3-type RAM and a 32-bit processor (model APL1012). This processor, called A8X, features a triple-core CPU at 1.5 GHz (Cyclone 2nd generation) with an ARMv8-A instructions set. All processes of signal acquisition, code detection, multipath cancellation, Gauss-Newton positioning and displaying of the results have been programmed in an Objective-C application with a total size of 1.1 MB, where approximately 1.3% (14 kB) corresponds to the source code of the MP algorithm. Programming all these processes in the iPad required an optimization effort to guarantee real-time operation, and the final app takes a maximum time of 223 ms to update the position without the MP algorithm and 674 ms when

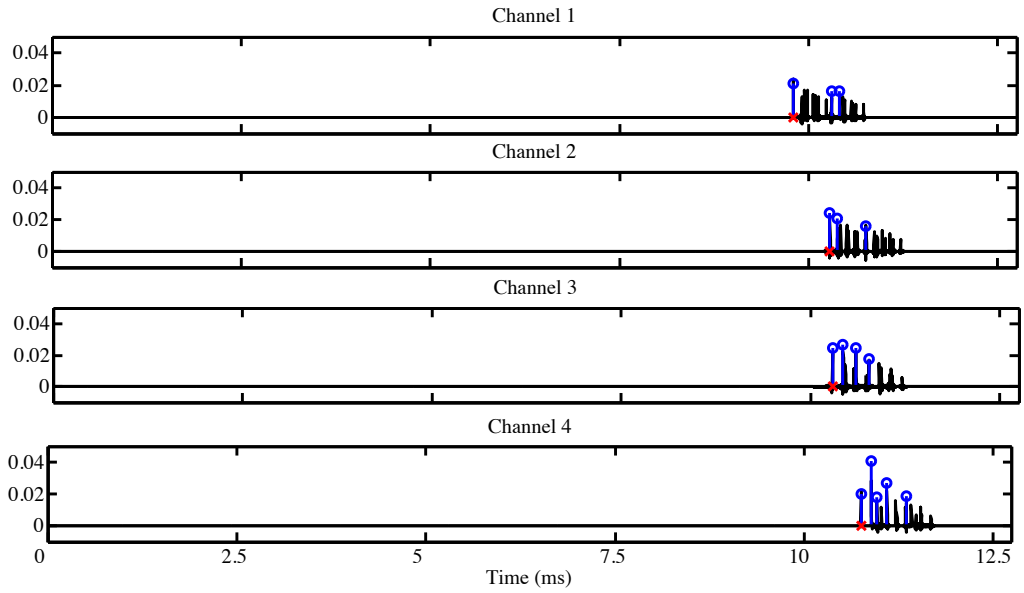


Figure 9: Impulsive response (black line), estimated coefficients (blue circles) and estimated LOS-TOF (red cross) under strong multipath interference conditions. The MP algorithm was programmed to calculate a minimum of three coefficients per channel.

this algorithm is activated. The operating block diagram showing all the processes involved in the positioning app is represented in Fig. 11.

Digital acquisition of an audio signal with an iOS device requires the configuration of the *Audio Queue Services*, which is a C programming interface in *Core Audio Toolbox* framework, available through *The Mac Developer Library* [50]. The audio signal acquisition rate was set to 96 kHz, thus giving a sampling / carrier frequency ratio of $F_s/F_c = 6$. The internal buffer size was set to 5556 samples, so the iPad's acquisition system takes 58 ms to complete its filling before the program saves these data from the buffer to a pointer in memory. The length of the signal acquisition window corresponds to the total length of two consecutive coded signal emissions (code+gap+code), which guarantees that this signal will be entirely captured inside the buffer at least once. Next, these samples are processed by means of the *vDSP API* which provides a wide family of DSP mathematical functions.

Finally, after all the signal processing tasks leading to an estimated position, this position is displayed to the user through a graphical interface designed for this purpose. Fig. 12 shows an

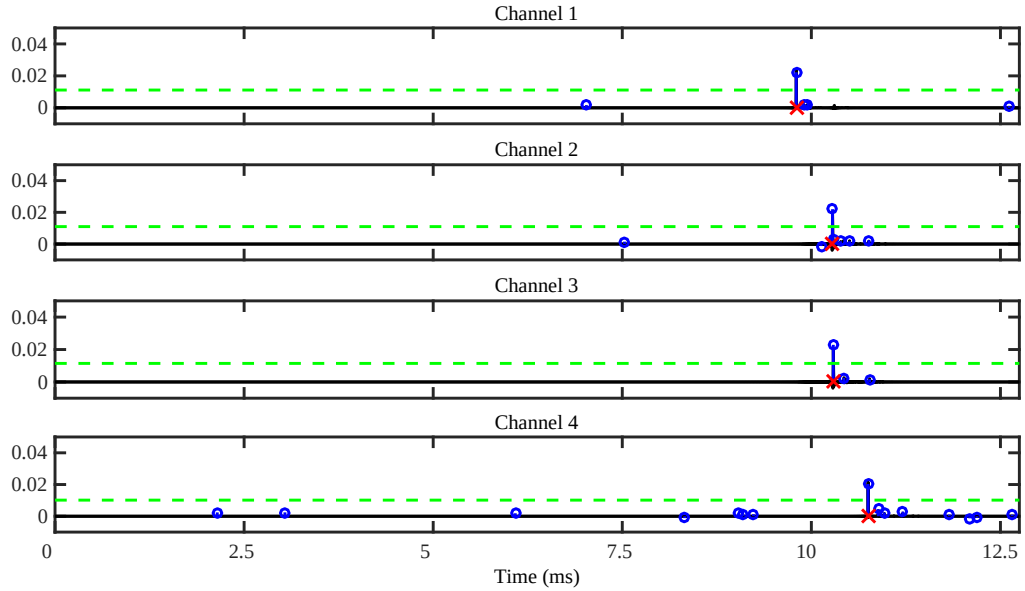


Figure 10: Impulsive response (black solid line), estimated coefficients (blue circles), detection threshold (green dashed line)

and estimated LOS-TOF (red cross) under weak multipath interference conditions. The MP algorithm was programmed to calculate a minimum of three coefficients per channel.

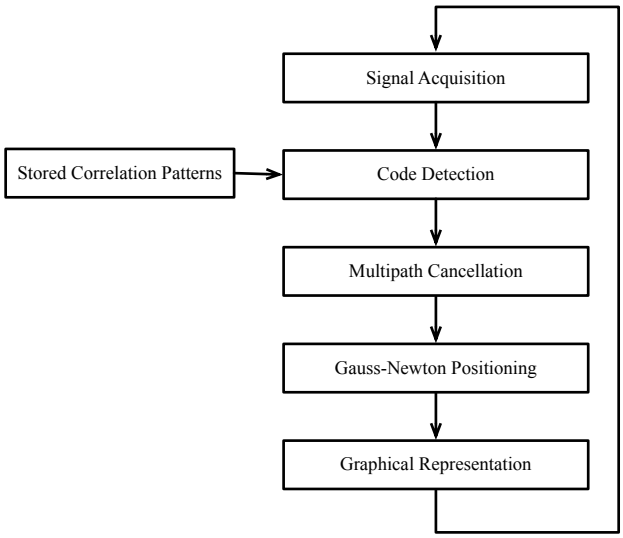


Figure 11: Block diagram of the whole iOS positioning app.

snapshot of this interface where we can see a map of the laboratory with the beacons location (black squares), a grid of test points (black dots) and the user's estimated position (red dot). This interface also incorporates Start/Stop and Exit buttons to manage the application, as well as a text box to introduce the current temperature that is used to adjust the sound speed value.

## 5. Experimental Results

### *5.1. System characterization*

Prior to analyzing the performance of the algorithm described in section 3, an experimental study has been conducted to characterize the proposed ALPS in terms of two parameters, namely, the Mean Positioning Error (MPE) and the System Availability (SA), the latter defined as the percentage of measurements whose error is below the outliers threshold (50 cm).

First, the system performance in different locations of the positioning area has been studied by fixing the portable device at an height of 1.1 m in each one of the 49 test points represented in Fig. 12, where it has been configured to continuously perform 200 location computations. The results of this study are shown in Fig. 13, where the SA is represented as a length in the z direction and the MPE is depicted using a color code. Hence, a good result (high SA with low MPE) corresponds to a long greenish bar, whereas a bad result (low SA with high MPE) is represented by a short reddish

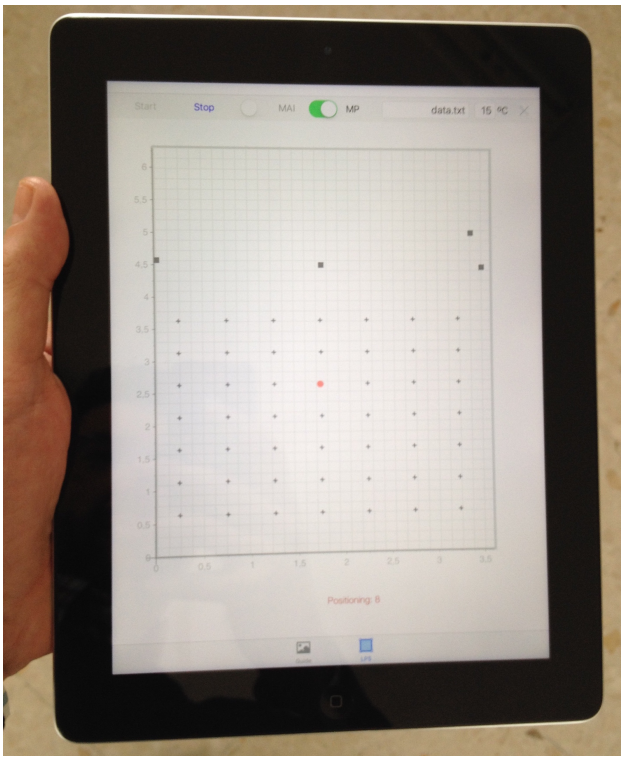


Figure 12: Screenshot of the user interface.

bar. As can be seen in this figure, the lowest values of SA (equal or very close to 0) are obtained in those tests points near the the wall with $x = 0$ coordinate, where strong echoes from the emissions of beacons B1 and B3 overlap with the direct emissions from all beacons. The largest positioning errors are obtained in the boundaries of the three walls. As expected, the best results are obtained in the center of the positioning area with SA above 90% and MPE below 8 cm.

Next, we have investigated the influence of the receiver's orientation on the system performance by fixing the iPad in the center of the positioning area with a precision tripod that allows for an accurate control of its pitch and yaw angles. Fig. 14a shows a picture of this tripod with the iPad, and Figs. 14 b and c show the results of this analysis for the SA and MPE respectively. As can bee seen in Fig. 14 b, the SA is very high with pitch angles between $-10^\circ$ and $15^\circ$ and with yaw angles between $-20^\circ$ and $5^\circ$, and it drops abruptly out of these ranges. The asymmetric behavior observed with respect to the yaw angle is a consequence of the beacon's distribution in this ALPS, since the emission from B1 is lost for yaw angles above $5^\circ$. Clearly, this behavior

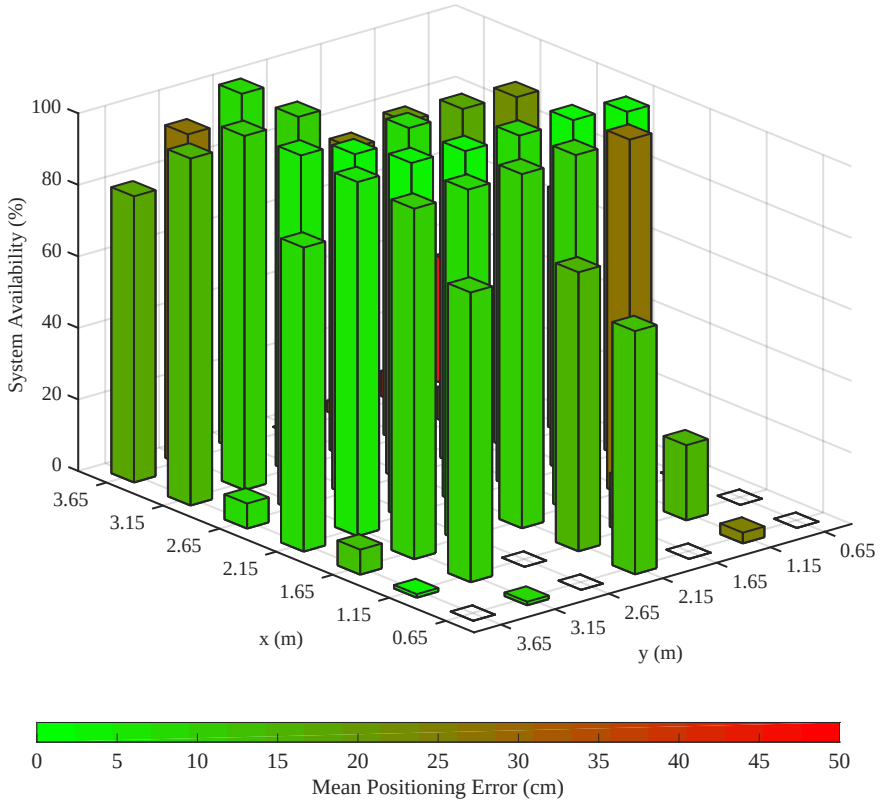


Figure 13: Mean positioning error (MSE) and System Availability (SA) of the system in the 49 test points of the positioning area.

could be easily improved by shifting the emplacement of B1 to a more centered position, at the expense of deteriorating the mean PDOP in the positioning area. Fig. 14 c shows that the lowest mean errors (ideal orientation) are obtained with pitch angles between $10^\circ$ and $15^\circ$ and yaw angles between $-5^\circ$ and $0^\circ$. The orientation of the iPad during the testing of performance in different locations (Fig. 13) was within these ranges.

Finally, it is also interesting to characterize the system behavior in terms of robustness against noise. Note that the emitted signals have most part of their energy in the high frequency audible range, so this system is intended to operate at very low SNR to make these emissions imperceptible to the human ear. In practice, the emission transients can be slightly heard, though, since they cause an increment of 7 dBA (from 40 to 47 dBA) in the A-weighted room noise level. To experimentally

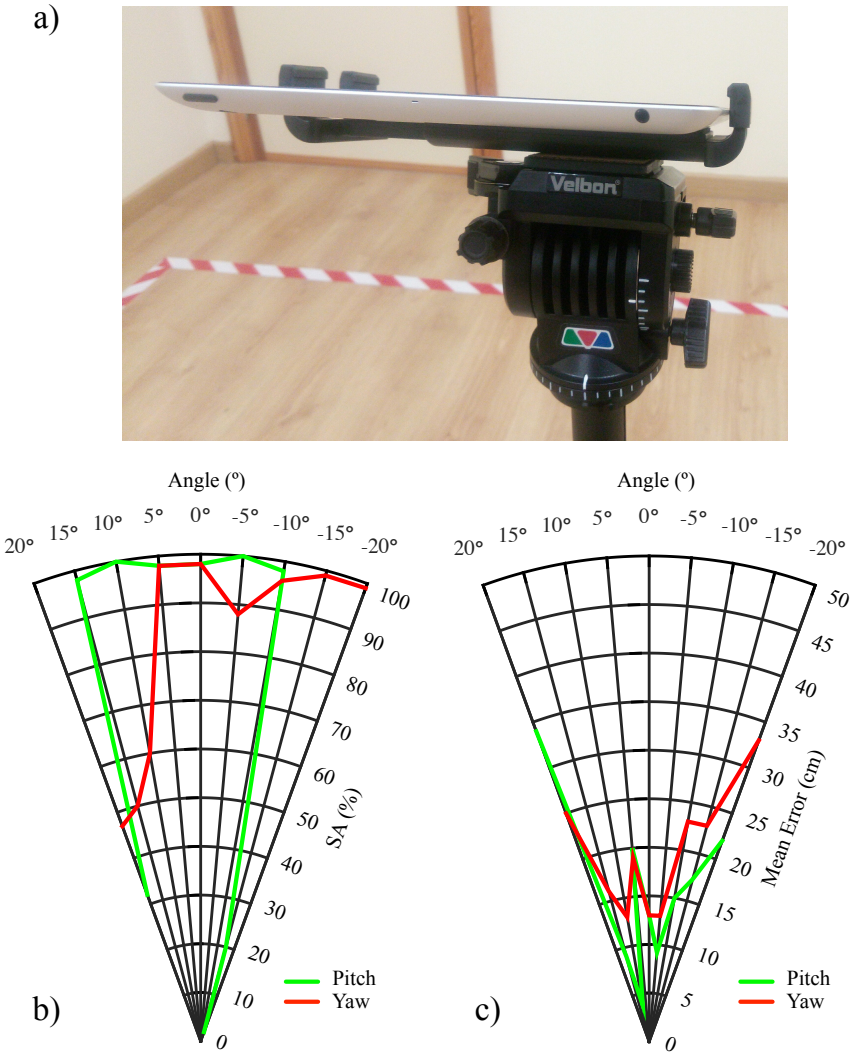


Figure 14: Influence of the receiver's orientation on the system performance: a) Picture of the precision tripod with the iPad, b) Dependence of SA with pitch and yaw angles and c) Dependence of MPE with these angles.

investigate this robustness, an additional beacon has been placed at coordinates ($x = 1.760$, $y = 4.4837$, $z = 1.160$) emitting Gaussian white noise with selectable power level. The receiver has been again fixed in the center of the positioning area with ideal orientation, and 200 locations computations has been performed in these conditions. The error distribution of these computations has been described in terms of their cumulative distribution function (CDF). Fig. 15 shows the

results obtained when the SNR is selected to be 12, 9, 6, 3, and 0 dBs, this SNR being defined as,

$$SNR = 10 \cdot \log \frac{P_s}{P_{ne} + P_{na}}, \tag{13}$$

where $P_s$ is the power of the emitted positioning signals, $P_{ne}$ is the power of the emitted noise, and $P_{na}$ is the power of the ambient noise measured in the absence of any emission. It is clear from Fig. 15 that noise increases the measurements dispersion, thus smoothing the CDFs slope to a lower value the higher the noise level.

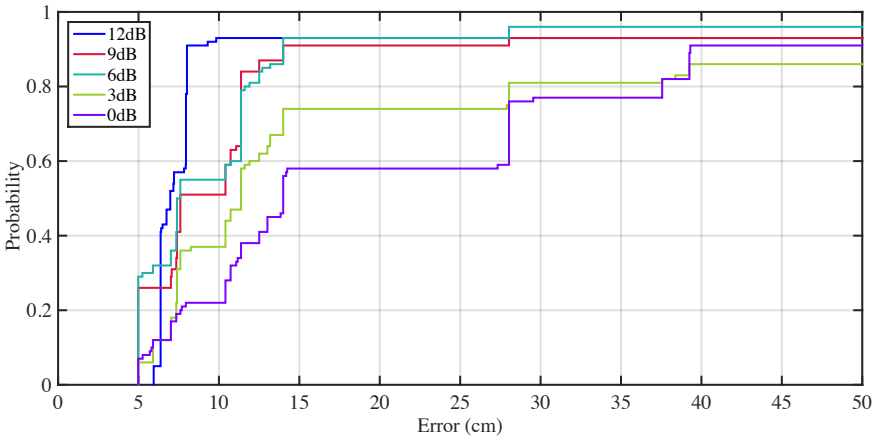


Figure 15: CDF of the positioning error in the absence of multipath at different SNR levels.

### *5.2. Performance of the multipath cancellation algorithm*

Once the behavior of the proposed ALPS has been characterized, a set of experiments have been conducted to evaluate the performance improvements associated with the use of the matching pursuit algorithm. Fig. 16 shows the SA and the MPE in the same 49 test points studied in Fig. 13, but when applying the multipath cancellation algorithm described in section 3. As can be seen, this algorithm retrieves a high percentage of measurements lost in the vicinity of the walls, and it also improves the MPE of these measurements, thus making the system useful in practice in the whole positioning area. Note that the largest errors are observed near to the wall which is further from the beacons location volume ($y = 0$), an expected result that is a consequence of the larger Dilution of Precision characterizing this region.

To further study the capability of the proposed algorithm to mitigate the effect of multipath propagation, a strong multipath has been forced in the center of the positioning area by placing

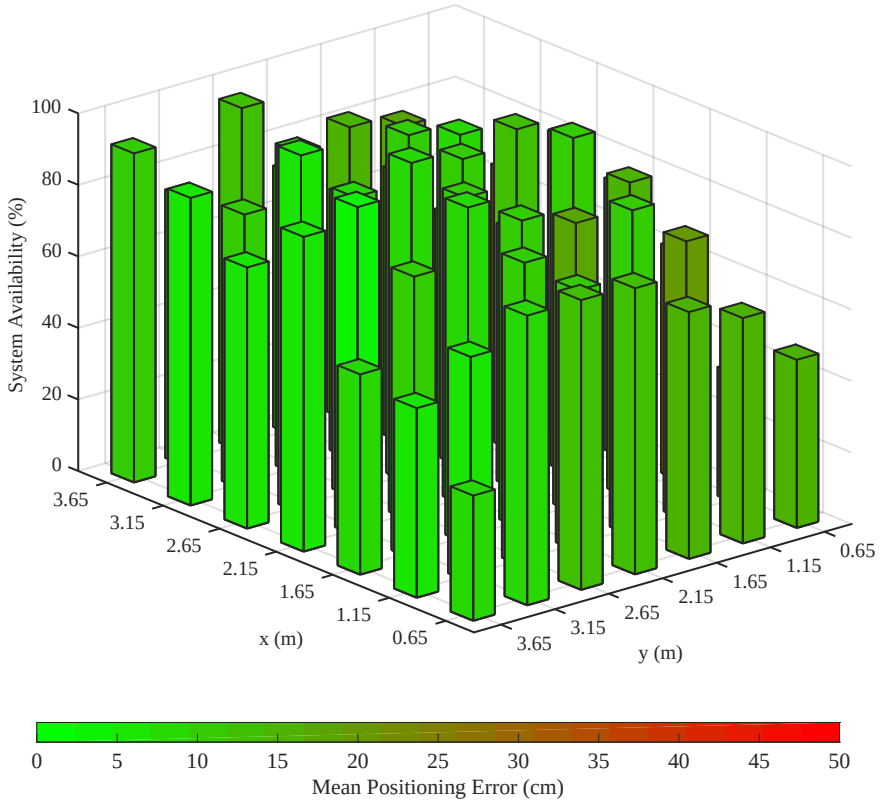


Figure 16: Mean positioning error (MPE) and System Availability (SA) of the system in the 49 test points of the positioning area after applying the MP algorithm.

a specular reflector (a cardboard box) at a distance of 30 cm from a receiver located in this ideal position. This distance is far below the product *emission duration* $\times$ *sound speed* $= 1.35$ m, a condition that ensures the reflected signals to overlap with the LOS receptions. Fig. 17 shows the results obtained in this scenario before and after applying the multipath cancellation algorithm. In the absence of the MP algorithm (dashed lines) the SA drops below 20%, with more than 80% of outliers. Note that a low number of precise measurements does not necessarily mean an inoperative system. It just indicates the need for an additional processing of the results to achieve a reliable final positioning. Needless to say, a deeper analysis of the error statistics is necessary to design the most adequate processing. In this case, and due to the presence of a permanent reflector, most outliers concentrate in the surroundings of a fixed erroneous position, which would make it

difficult for the system to discriminate between these and the correct measurements through the temporal filter described in Section 2.3. As can be seen in Fig. 17, this situation is solved by applying the proposed MP algorithm (solid line), which makes the SA to raise up to 91%, with a maximum error below 9.9 cm.

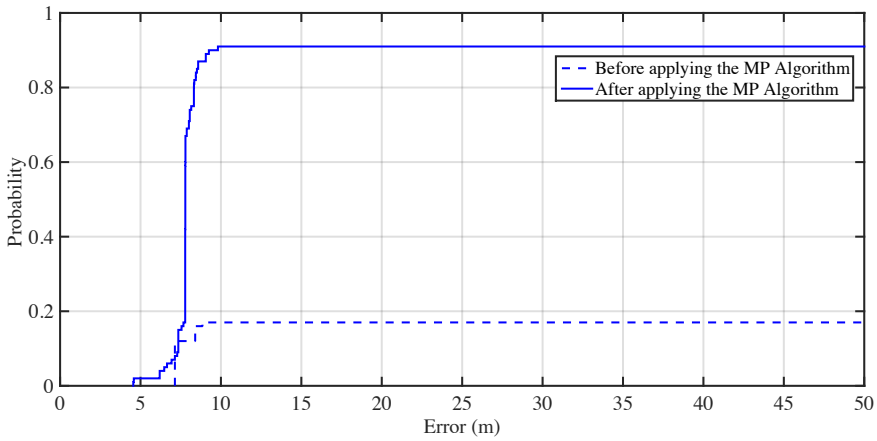


Figure 17: CDF of the positioning error under strong multipath, before (dashed) and after (solid) applying the MP algorithm.

The same study has been conducted with different levels of noise, generated as described in the previous section. As can be seen in Fig. 18, without the MP algorithm, all CDFs drop to a SA value below 20% (dashed lines). This figure also shows the results obtained when applying the MP algorithm for every SNR situation (solid lines). By comparing the solid lines in Figs. 15 and 18 we can see that the algorithm is retrieving most measurements with an error below 12 cm, and above this value, only measurements with very large errors or even divergences of the positioning algorithm are obtained. These valid measurements can be used to characterize the system accuracy through the mean and standard deviation of their error as summarized in Table 1, from where a system accuracy slightly below 8 cm can be inferred.

## 6. Conclusions

This work has presented an acoustic local positioning system (ALPS) suitable for indoor positioning of portable devices such as smartphones or tablet computers, and based on the transmission of high frequency CDMA-coded signals from a fixed beacon network to a mobile device.

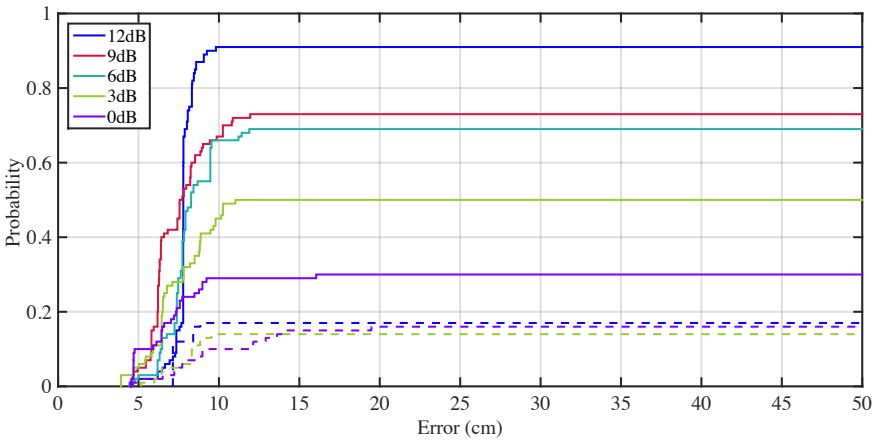


Figure 18: CDF of the positioning error under strong multipath with (solid) and without (dashed) the MP algorithm at different SNR levels.

| SNR (dB) | SA (%) | MPE (cm) | std (cm) |
|---|---|---|---|
| 12 | 91 | 7.8 | 0.7 |
| 9 | 73 | 7.1 | 1.6 |
| 6 | 69 | 7.8 | 1.4 |
| 3 | 50 | 7.3 | 1.8 |
| 0 | 29 | 6.5 | 1.6 |

Table 1: Positioning error results at different SNR levels: System Availability (SA), Mean Positioning Error (MPE) and standard deviation of this error.

The most remarkable novelty of the proposed ALPS is its capability to mitigate the effects of multipath propagation by performing an accurate estimation of the Line-of-Sight Time-of-Flights (LOS-TOF). This estimation makes use of the Matching Pursuit algorithm to calculate a minimum of three coefficients from the channel impulse responses, and obtains the desired LOS-TOF as the time of occurrence of the first coefficient whose value is above half the value of the largest coefficient estimated in each channel.

All processes involved in the positioning task, namely, signal detection, multipath cancellation, Gauss-Newton positioning and graphical representation of the results, have been implemented on a last generation iOS device (iPad Air 2) to operate at real time with a minimum position update

rate of 1.5 Hz.

The system performance has been characterized in terms of System Availability, i.e., the total percentage of valid measurements, and the Mean Positioning Error of these measurements. The dependence of this performance with receiver's location, receiver's orientation and level of noise has been analyzed in detail. Finally, the improvements associated with the use of the proposed multipath cancellation algorithm have been experimentally studied both in the boundaries of the positioning area and also by forcing a strong multipath in the center of this area. In the first case, results show that the algorithm is capable to retrieve a high percentage of measurements lost in the vicinity of the walls, thus making the system useful in practice in the whole positioning area. In the second case, it has been demonstrated that the proposed method is capable to retrieve the original System Availability under strong multipath condition with SNR levels ranging from 12 to 0 dB.

Further study should be conducted to investigate the performance of the proposed ALPS in other environments with different sizes, levels of noise and reverberation time.

## Acknowledgements

This work was funded by the Spanish Government and the European Regional Development Fund (ERDF) under projects TARSIUS (TIN2015-71564-C4-4-R), COMPASS (TEC2013-47020-C2-1-R) and COMONSENS (TEC2015-69648-REDC), by the Regional Government of Extremadura and ERDF under projects IB13065 and GR15167, and the Regional Government of Galicia and ERDF under projects GRC2013/009, R2014/037 and AtlantTIC.

[1] P. Zandbergen, Accuracy of iPhone Locations: A Comparison of Assisted GPS, WiFi and Cellular Positioning, Transactions in GIS 13 (2009) 5–26.

[2] H. Liu, H. Darabi, P. Banerjee, J. Liu, Survey of wireless indoor positioning techniques and systems, Systems, Man, and Cybernetics, Part C: Applications and Reviews, IEEE Transactions on 37 (6) (2007) 1067–1080.

[3] R. Mautz, Indoor Positioning Technologies, Institute of Geodesy and Photogrammetry, Department of Civil, Environmental and Geomatic Engineering, ETH Zurich, 2012.

[4] A. Dekel, E. Schiller, Drec: Exploring indoor navigation with an un-augmented smart phone, in: Proceedings of the 12th International Conference on Human Computer Interaction with Mobile Devices and Services, MobileHCI '10, 2010, pp. 393–394.

[5] J. Link, P. Smith, N. Viol, K. Wehrle, Footpath: Accurate map-based indoor navigation using smartphones, in: Indoor Positioning and Indoor Navigation (IPIN), 2011 International Conference on, 2011, pp. 1–8.

[6] T. Shanklin, B. Loulier, E. Matson, Embedded sensors for indoor positioning, in: Sensors Applications Symposium (SAS), 2011 IEEE, 2011, pp. 149–154.

[7] W. Kang, S. Nam, Y. Han, S. Lee, Improved heading estimation for smartphone-based indoor positioning systems, in: Personal Indoor and Mobile Radio Communications (PIMRC), 2012 IEEE 23rd International Symposium on, 2012, pp. 2449–2453.

[8] F. Li, C. Zhao, G. Ding, J. Gong, C. Liu, F. Zhao, A reliable and accurate indoor localization method using phone inertial sensors, in: Proceedings of the 2012 ACM Conference on Ubiquitous Computing, UbiComp '12, 2012, pp. 421–430.

[9] K. Wendlandt, M. Berhig, P. Robertson, Indoor localization with probability density functions based on bluetooth, in: Personal, Indoor and Mobile Radio Communications, 2005. PIMRC 2005. IEEE 16th International Symposium on, Vol. 3, 2005, pp. 2040–2044.

[10] M. Rodriguez, J. P. Pece, C. J. Escudero, In-building location using bluetooth, in: in In Proceedings of the International Workshop on Wireless Ad Hoc Networks, 2005.

[11] S. Subramanian, J. Sommer, S. Schmitt, W. Rosenstiel, SBIL: Scalable indoor localization and navigation service (2007) 27–30.

[12] W. Muttitanon, N. K. Tripathi, M. Souris, An indoor positioning system (IPS) using grid model, Journal of Computer Science 3 (12) (2007) 907–913.

[13] T. Gallagher, B. Li, A. G. Dempster, C. Rizos, A sector-based campus-wide indoor positioning system, in: Indoor Positioning and Indoor Navigation (IPIN), 2010 International Conference on, 2010, pp. 1–8.

[14] J. Ledlie, P. Jun-geun, D. Curtis, A. Cavalcante, L. Camara, A. Costa, R. Vieira, Mole: A scalable, user-generated WiFi positioning engine, in: Indoor Positioning and Indoor Navigation (IPIN), 2011 International Conference on, 2011, pp. 1–10.

[15] C. Laoudias, G. Constantinou, M. Constantinides, S. Nicolaou, D. Zeinalipour-Yazti, C. G. Panayiotou, The airplace indoor positioning platform for android smartphones, in: Proceedings of the 2012 IEEE 13th International Conference on Mobile Data Management (Mdm 2012), MDM '12, IEEE Computer Society, Washington, DC, USA, 2012, pp. 312–315.

[16] J. Liu, R. Chen, L. Pei, W. Chen, T. Tenhunen, H. Kuusniemi, T. Kroger, Y. Chen, Accelerometer assisted robust wireless signal positioning based on a hidden markov model, in: Position Location and Navigation Symposium (PLANS), 2010 IEEE/ION, 2010, pp. 488–497.

[17] C. Wu, Z. Yang, Y. Liu, W. Xi, WILL: Wireless Indoor Localization without Site Survey, in: INFOCOM, 2012 Proceedings IEEE, 2012, pp. 64–72.

[18] J. Liu, R. Chen, L. Pei, R. Guinness, H. Kuusniemi, A Hybrid Smartphone Indoor Positioning Solution for

Mobile LBS, Sensors 12 (12) (2012) 17208–17233.

[19] T. Gallagher, E. Wise, B. Li, A. Dempster, C. Rizos, E. Ramsey-Stewart, Indoor positioning system based on sensor fusion for the blind and visually impaired, in: Indoor Positioning and Indoor Navigation (IPIN), 2012 International Conference on, 2012, pp. 1–9.

[20] L. Pei, J. Liu, R. Guinness, Y. Chen, H. Kuusniemi, R. Chen, Using LS-SVM based motion recognition for smartphone indoor wireless positioning, Sensors 12 (5) (2012) 6155–6175.

[21] A. Bahillo, J. Prieto, H. Fernández, P. Fernández, R. Lorenzo, E. Abril, Fusing Technologies for a Continuous Positioning Solution Developed on a Smartphone, in: Computing and Convergence Technology (ICCCT), 2012 7th International Conference on, 2012, pp. 763–766.

[22] A. Mandal, C. Lopes, T. Givargis, A. Haghighat, R. Jurdak, P. Baldi, Beep: 3D Indoor Positioning using Audible Sound, in: Consumer Communications and Networking Conference, 2005. CCNC. 2005 Second IEEE, 2005, pp. 348–353.

[23] C. V. Lopes, A. Haghighat, A. Mandal, T. Givargis, P. Baldi, Localization of Off-the-shelf Mobile Devices Using Audible Sound: Architectures, Protocols and Performance Assessment, SIGMOBILE Mob. Comput. Commun. Rev. 10 (2) (2006) 38–50.

[24] V. Filonenko, C. Cullen, J. Carswell, Investigating Ultrasonic Positioning on Mobile Phones, in: Indoor Positioning and Indoor Navigation (IPIN), 2010 International Conference on, 2010, pp. 1–8.

[25] V. Filonenko, C. Cullen, J. D. Carswell, Indoor Positioning for Smartphones Using Asynchronous Ultrasound Trilateration, ISPRS International Journal of Geo-Information 2 (3) (2013) 598–620.

[26] C. Peng, G. Shen, Y. Zhang, Y. Li, K. Tan, BeepBeep: A High Accuracy Acoustic Ranging System Using COTS Mobile Devices, in: Proceedings of the 5th International Conference on Embedded Networked Sensor Systems, SenSys '07, ACM, New York, NY, USA, 2007, pp. 1–14.

[27] B. Xu, R. Yu, G. Sun, Z. Yang, Whistle: Synchronization-Free TDOA for Localization, in: Distributed Computing Systems (ICDCS), 2011 31st International Conference on, 2011, pp. 760–769.

[28] J. Qiu, D. Chu, X. Meng, T. Moscibroda, On the Feasibility of Real-Time Phone-to-Phone 3D Localization, in: Proceedings of ACM SenSys 2011, ACM SenSys, 2011.

[29] J.-W. Qiu, C. C. Lo, C.-K. Lin, Y.-C. Tseng, A D2D Relative Positioning System on Smart Devices, in: IEEE Wireless Communications and Networking Conf. (WCNC), 2014.

[30] A. J. Bianchi, M. Queiroz, On the Performance of Real-Time DSP on Android Devices, in: Proceedings of the 9th Sound and Music Computing Conference, 2012, pp. 113–120.

[31] M. Hazas, A. Hopper, Broadband Ultrasonic Location Systems for Improved Indoor Positioning, Mobile Computing, IEEE Transactions on 5 (5) (2006) 536–547.

[32] J. R. González, C. J. Bleakley, High-precision robust broadband ultrasonic location and orientation estimation, IEEE Journal of selected topics in Signal Processing 3 (5) (2009) 832–844.

[33] J. C. Prieto, A. R. Jiménez, J. Guevara, J. L. Ealo, F. Seco, J. O. Roa, F. Ramos, Performance evaluation of 3D-Locus advanced acoustic LPS, IEEE Trans. on Instrumentation and Measurement 58 (8) (2009) 2385–2395.

[34] F. J. Álvarez, A. Hernández, J. A. Moreno, M. C. Pérez, J. Ureña, Doppler-tolerant receiver for an ultrasonic LPS based on Kasami sequences, Sensors and Actuators A: Physical (2013) 238–253.

[35] D. B. Haddad, W. A. Martins, M. V. M. da Costa, L. W. P. Biscainho, L. O. Nunes, B. Lee, Robust Acoustic Self-Location of Mobile Devices, IEEE Transactions on Mobile Computing 15 (4) (2016) 982–995.

[36] M. Cobos, J. J. Pérez-Solano, O. Belmonte, G. Ramos, A. M. Torres, Simultaneous Ranging and Self-Positioning in Unsynchronized Wireless Acoustic Sensor Networks, IEEE Transactions on Signal Processing 64 (22) (2016) 5993–6004.

[37] R. A. Iltis, S. Kim, Geometric derivation of expectation-maximization and generalized succesive interference cancellation algorithms with applications to CDMA channel estimation, IEEE Transactions on Signal Processing 51 (5) (2003) 1367–1377.

[38] S. Kim, R. A. Iltis, A matching-pursuit/GSIC-based algorithm for DS-CDMA sparse-channel estimation, IEEE Signal Processing Letters 11 (1) (2004) 12–15.

[39] F. J. Álvarez, R. López-Valcarce, Multipath Cancellation in Broadband Acoustic Local Positioning Systems, in: Intelligent Signal Processing (WISP), 9th IEEE International Symposium on, 2015, pp. 124–129.

[40] J. B. Allen, D. A. Berkley, Image method for efficiently simulating small-room acoustics , Journal of the Acoustical Society of America 65 (4) (1979) 943–950.

[41] H. Azami, M.-R. Mosavi, S. Sanei, Classification of GPS Satellites Using Improved Back Propagation Training Algorithms, Wireless Personal Communications 71 (2013) 789–803.

[42] M. R. Schroeder, Integrated-Impulse Method for Measuring Sound Decay without Using Impulses, Journal of the Acoustical Society of America 66 (1979) 497–500.

[43] J. Ureña, A. Hernández, J. M. Villadangos, M. Mazo, J. C. García, J. J. García, F. J. Álvarez, C. Marziani, M. C. Pérez, J. A. Jiménez, A. Jiménez, F. Seco, Advanced sensorial system for an acoustic LPS, Microprocessors and Microsystems 31 (2007) 393–401.

[44] E. García, J. Ureña, J. García, M. C. Pérez, F. D. Ruiz, C. Diego, J. Aparicio, Multilevel LS Sequences with Flexible ZCZ Length and their Application to Local Positioning Systems, in: Instrumentation and Measurement Technology Conference, (I2MTC), 2012 IEEE International, 2012, pp. 1665–1669.

[45] J. A. Paredes, T. Aguilera, F. J. AÍvarez, J. Lozano, J. Morera, Analysis of doppler effect on the pulse compression of different codes emitted by an ultrasonic LPS, Sensors 11 (2011) 10765–10784.

[46] J. G. Proakis, Digital Communications, 4th Edition, McGraw-Hill, 2000.

[47] W. H. Foy, Position-Location Solutions by Taylor-Series Estimation, IEEE Trans. Aerospace and Electronic Systems AES-12 (2) (1976) 187–194.

[48] P. Stoica, J. Li, Source localization from range-difference measurements, IEEE Signal Processing Magazine

23 (69) (2006) 63–65.

[49] M. A. Sturza, Navigation System Integrity Monitoring using Redudant Meaurements, Journal of the Institute of Navigation 35 (4) (1988) 69–87.

[50] https://developer.apple.com/xcode/ (2014).